RECENT DEVELOPMENTS WITH THE GTS-LHC ECR ION SOURCE AT CERN

V. Toivanen*, G. Bellodi, C. Fichera, D. Küchler, A. M. Lombardi,
M. Maintrot, A. Michet, M. O'Neil, S. Sadovich, F. Wenander
European Organization for Nuclear Research (CERN), Geneva, Switzerland
O. Tarvainen, University of Jyväskylä, Department of Physics (JYFL), Jyväskylä, Finland

Abstract

Linac3 is the first link in the chain of accelerators providing highly charged heavy ion beams for the CERN experimental program. The beams, predominantly lead, are produced with the GTS-LHC 14.5 GHz Electron Cyclotron Resonance (ECR) ion source, operated in afterglow mode. In the framework of the LHC Injector Upgrade program (LIU), several activities have been carried out to improve the GTS-LHC and Linac3 performance, in terms of delivered beam current.

The extraction region of the GTS-LHC has been upgraded with redesigned apertures and the addition of an einzel lens, yielding improved Linac3 output. Also, a series of measurements has been performed to study the effects of double frequency heating on the afterglow performance of the GTS-LHC. A Travelling Wave Tube Amplifier (TWTA) with variable frequency and pulse pattern was utilized as a secondary microwave source. The double frequency effect commonly reported with CW operation of ECR ion sources boosting high charge state ion production was also observed in afterglow mode. Lastly, for studies of metal ion beam production, a dedicated test stand has been assembled to characterize the GTS-LHC resistively heated miniature oven performance.

INTRODUCTION

In order to prepare for the future high luminosity operation of the Large Hadron Collider (LHC), all the accelerators providing beam for the LHC experiments are undergoing an extensive upgrade program; the LHC Injector Upgrade (LIU). For the heavy ion accelerator chain this includes, from the lowest beam energy to the highest, the Linac3 linear accelerator, the Low Energy Ion Ring (LEIR), the Proton Synchrotron (PS) and the Super Proton Synchrotron (SPS). As part of the Linac3 upgrades, several activities have been carried out with the GTS-LHC Electron Cyclotron Resonance (ECR) ion source [1], which produces the primary heavy ion beams for the CERN experiments.

GTS-LHC is a 14.5 GHz second generation ECR ion source which is based on the Grenoble Test Source (GTS) by CEA, Grenoble [2]. The main differences to the GTS include a modified magnetic field structure with an added center coil and a stronger Halbach-style 36-piece permanent magnet hexapole. GTS-LHC is exclusively operated in afterglow mode to produce mainly lead ion beams, although also argon beam was delivered for experiments in 2015 and xenon is planned for 2017. The afterglow operation is performed with a 10 Hz RF heating cycle at 50 % duty factor. A ~200 µs ion beam pulse is selected and accelerated through the linac from the afterglow burst which is exhibited by the extracted ion beam after the microwave switch-off. The lead beam is produced as $^{208}Pb^{29+}$ with 2.5 keV/u initial energy, as it provides the highest particle current during afterglow, and is stripped to $^{208}Pb^{54+}$ at the end of the linac for injection into LEIR with 4.2 MeV/u energy.

This paper presents three activities that have been recently carried out with the GTS-LHC; the GTS-LHC extraction region upgrade, double frequency plasma heating combined with afterglow operation and oven studies for metal ion beam production. These topics are discussed in the following chapters.

EXTRACTION REGION UPGRADE

Following a dedicated simulation study [3–5] the beam extraction region of the GTS-LHC was modified in the beginning of 2016. The goal of this upgrade was to increase the beam currents out of Linac3 by mitigating the beam losses immediately after the ion source and by improving the flexibility of the ion source tuning and matching to the following low energy beam transport (LEBT) section.

One of the main issues of the original extraction system that was observed with the simulations and verified with inspection of the extraction chamber was the strong divergence of the extracted ion beams. Due to the limited tuning capabilities of the extraction system this resulted in the collimation of a significant part of the extracted ion beam at the entrance of the beam pipe at the end of the ion source extraction chamber [4]. In order to improve the beam transmission in this region, the section immediately downstream from the extraction electrodes was redesigned with two main modifications. Firstly, in order to improve the transport flexibility and to mitigate beam collimation, the aperture restrictions were relaxed by increasing the beam pipe bore through the first beam line solenoid from 65 to 100 mm. Secondly, a new bipolar einzel lens was installed inside the extraction chamber to provide additional beam focusing and matching to the following beam transport section. A comparison of the original and the upgraded extraction regions are presented in Fig. 1. Further details of the designs are given in Ref. [5].

The performance of Linac3 has improved steadily after the implementation of the extraction region upgrade, as experience has been gained on how to optimize the ion source matching to the new beam transport conditions. The present

* ville.aleksi.toivanen@cern.ch

ISBN 978-3-95450-186-1

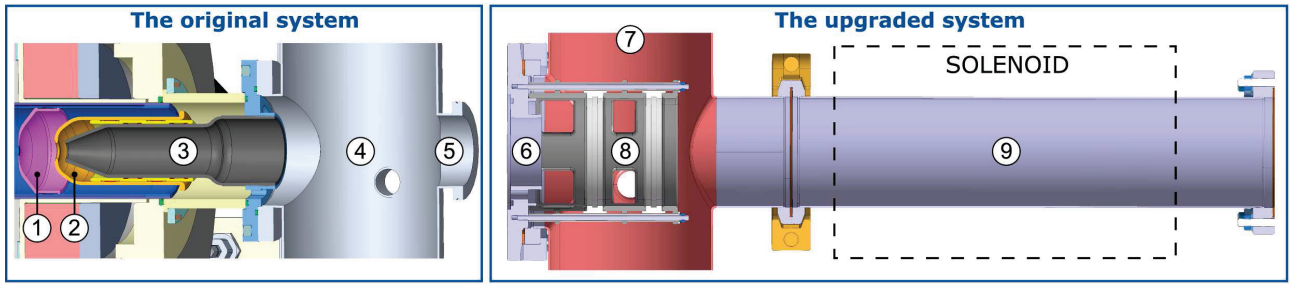

Figure 1: Comparison of the original and the upgraded GTS-LHC extraction regions. In the original design the intermediate (2) and grounded electrodes (3) are supported in front of the plasma electrode (1) on a flange which is connected to the extraction chamber (4). The chamber is followed by a 65 mm diameter beam pipe (5). In the upgraded system the flange (6) and the extraction chamber (7) have been redesigned to allow the installation of an einzel lens (8) and a larger 100 mm diameter beam pipe through the first beam line solenoid (9).

Table 1: Comparison of typical lead beam currents from the ion source and out of Linac3 before and after the extraction region upgrade. The values for the original system before upgrade are from the 2015 lead run.

Ion species and location	*Original system (2015 run)*	*Upgraded system*	*Improvement*
$^{208}Pb^{29+}$ from the ion source	170 µA	210 µA	24 %
$^{208}Pb^{54+}$ out of Linac3	25 µA	35 µA	40 %

performance with lead downstream from the ion source and at the output of Linac3 is presented in Table 1. Compared to the 2015 lead run, the beam currents of $^{208}Pb^{29+}$ delivered from the ion source through the spectrometer have increased over 20 %, and the Linac3 output current for $^{208}Pb^{54+}$ is up to 40 % higher than before. The increased flexibility in the ion source tuning allows operation with different source settings than before without compromising the beam transmission. This has led to improved beam stability and matching to the rest of the linac, as is evident from the fact that the linac output current exhibits greater improvement than the current out of the ion source.

DOUBLE FREQUENCY OPERATION IN AFTERGLOW MODE

Using multiple discrete frequencies simultaneously for ECR plasma heating is a well-established method to improve ECR ion source performance with high charge state ion beam production (see e.g. Refs. [6, 7]). However, the experiments with multiple frequencies have been mainly performed with ECR ion sources operated in CW mode, and especially detailed data with afterglow operation is not readily available. As this is the main operation mode to produce beams at Linac3, a set of experiments have been performed to study the effects of double frequency heating on the afterglow performance of GTS-LHC. A comprehensive description of the studies is reported in Ref. [8].

The measurement setup used in the experiments is presented in Fig. 2. The microwave radiation at the primary 14.5 GHz frequency is delivered from a klystron amplifier through a WR62 rectangular wave guide assembly. In normal operation the klystron is operated in pulsed mode at 10 Hz repetition rate and 50 % duty factor, providing ~2 kW of power during the RF pulse. The secondary WR62 wave guide of the ion source, normally used for a spare 14.5 GHz klystron, was connected to a Travelling Wave Tube Amplifier (TWTA) to provide microwaves at a variable secondary frequency. The transmission and reflection characteristics of the HV break and the vacuum window between the TWTA and the plasma chamber were measured to determine the limits for the frequencies that could pass through the system. As a result, the frequency range for the secondary microwaves was limited to 12–18 GHz. For these frequencies the maximum power delivered from the amplifier was ~300 W. A directional isolator was installed at the output of the TWTA to protect it from the pulsed main microwave radiation. The input signal was generated with a variable frequency oscillator driven with a digital pulse and delay generator. The pulse generator was triggered by the klystron timing signal, allowing pulsed operation of the TWTA with respect to the klystron pulse pattern, as well as CW operation.

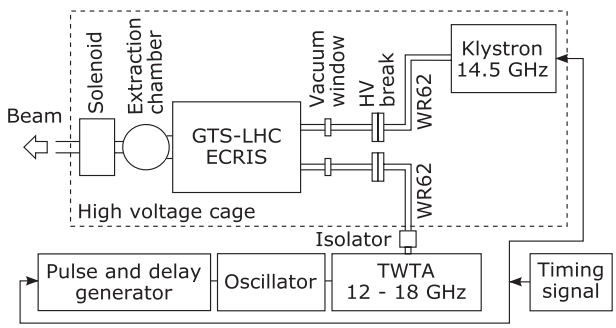

Figure 2: A schematic presentation of the double frequency measurement setup at Linac3.

ISBN 978-3-95450-186-1

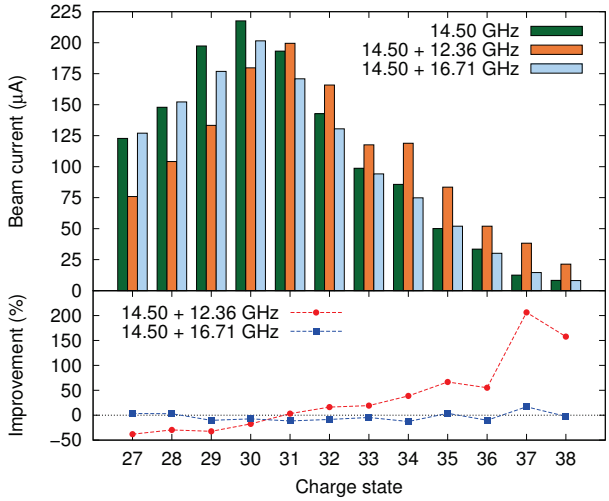

Figure 3: Top: Afterglow CSDs measured with single and double frequency operation. Klystron output at 1920 W, TWTA at 180 W and 185 W for 12.36 GHz and 16.71 GHz, respectively. Bottom: Beam current improvements with two frequencies compared to the single frequency case.

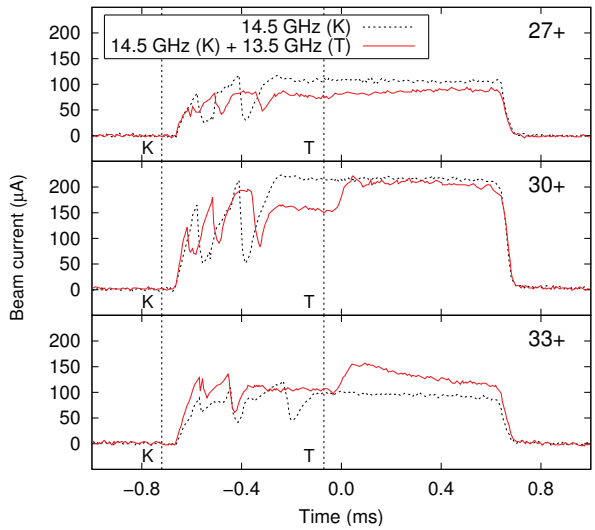

Figure 4: Beam currents of Pb^{27+}, Pb^{30+} and Pb^{33+} with single and double frequency heating. 13.50 GHz secondary frequency with 0.65 ms trailing edge delay (indicated with the dashed vertical lines for klystron (K) and TWTA (T)). To avoid beam-loss induced interference with the linac RF systems, the steady state part of the beam pulse at $t < -0.68$ ms and the tail of the afterglow at $t > 0.63$ ms have been actively removed from the beam pulse.

When both the primary and the secondary microwave sources are pulsed synchronously and a suitable secondary frequency is chosen, a shift to higher charge states was observed in the charge state distribution (CSD) measured during the afterglow. Concerning the frequency dependency of this effect, the shift in CSD was in general seen when the secondary frequency was chosen to be lower than the primary one, whereas with higher frequencies the influence to the beam currents was significantly weaker and no clear shift was evident in the measured data. An example of this is presented in Fig. 3. It was verified that the shift to higher charge states is not simply due to increased total microwave power, as this effect was observed also when the combined power in double frequency operation was matched with the power level used in the single frequency case. However, an increase in the total power in the double frequency case does provide a further improvement for the high charge states.

Introducing a time delay between the trailing edges of the primary and the secondary microwave pulses leads the afterglow current to exhibit a second step-like increase following the switch-off of the TWTA. This reflects the two-stage collapse of the plasma, indicating that part of the ion population remains trapped until the secondary microwaves are switched off. Figure 4 showcases this current behaviour for selected lead charge states.

When the TWTA is switched to CW mode while keeping the klystron pulsed, an afterglow burst is still observed after the trailing edge of the primary microwave pulse, but the beam current during the discharge is reduced compared to pulsing of both frequencies. This mitigation is explained by the secondary microwaves sustaining the plasma between the primary microwave pulses and consequently part of the ion population is constantly retained inside the trap.

Pb^{29+} was studied in more detail, as it is the primary beam from GTS-LHC. Best response was observed with 14.2 GHz pulsed secondary frequency, yielding beam current improvements in the order of $10 - 20$ % after the source.

With the ion source solenoid settings used in the experiments, the lowest value of the minimum B field inside the plasma chamber was 0.47 T, which corresponds to a lower limit of 13.16 GHz for the microwave frequencies that fulfil the electron cyclotron resonance condition for non-relativistic electrons. This limit excludes the frequencies around 12.36 GHz which experimentally provided the best improvement to the high charge state beam currents. For these frequencies the resonance only exists for electrons with energies >30 keV. Further heating of this population should not directly improve the ionization efficiency of the measured ion species, because these electron energies are significantly higher than the energies corresponding to the maxima of the electron impact ionization cross section for the lead charge states in question (<8 keV [9, 10]). However, it is noted that improved performance with secondary off-resonance frequencies has recently also been reported with CW operation [11]. It has been suggested that this effect is caused by suppression of plasma instabilities through the interaction of the secondary microwave radiation with the hot electron population in the plasma. However, further studies are required to identify the exact mechanisms behind this observed behaviour.

ISBN 978-3-95450-186-1

MINIATURE OVEN STUDIES

The lead ion beams delivered by Linac3 are produced with GTS-LHC using resistively heated miniature ovens. The oven design consists of an aluminium oxide crucible, tantalum heating filament, tantalum oven body and stainless steel cane to allow axial insertion through the ion source injection plug. The oven structure is presented in Fig. 5.

The GTS-LHC features two oven ports through the injection plug. In normal operation the two ovens provide 2 – 3 weeks of lead beam operation between refills. However, it has been observed that when refill is required due to degrading beam performance, typically about 2/3 of the lead is still left in the oven. In some instances the operation is also interrupted by blockage of the oven tip, either by formation of lead oxide or droplets of metallic lead. In order to study the oven performance and failure mechanisms in more detail, a dedicated offline test stand has been constructed with capabilities to measure the oven temperatures and lead evaporation rates in varied input power and vacuum or gas atmosphere conditions. The lead evaporation from the oven is measured using an INFICON surface deposition detector with quartz crystal sensor. Temperature measurement are primarily performed with vacuum grade thermocouples. ZnSe viewports with high infrared transmission are an additional option for temperature monitoring with a thermal camera and borosilicate viewports are used for visual inspection during measurements.

Figure 6 presents a temperature characterization of the oven, measured in the test stand. For lead beam production the oven is normally operated with power levels above 6 W, which translates to temperatures over 600 °C based on the measurement. With 20 W, which is the maximum power used in operation, the temperature inside the crucible reaches about 950 °C. It is observed that the measured oven temperatures T follow a $T \propto P^{1/4}$ relationship, where P is the oven input power. This indicates that radiative losses dominate the oven thermal behaviour. In addition, the measurements have shown that the oven is slow to respond to input power changes, and several hours are required to reach temperature equilibrium at lower power levels. This delayed response is also observed in GTS-LHC operation.

The normalized lead evaporation rate is presented in Fig. 7 as a function of the crucible temperature. The measured data shows steady response in the lead output and the observed temperature dependency agrees well with the shape

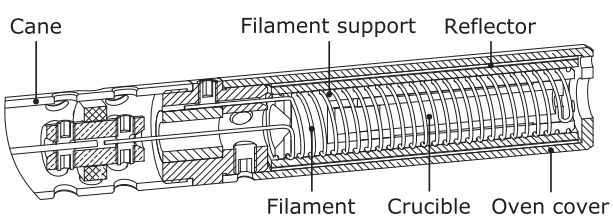

Figure 5: A schematic of the GTS-LHC miniature oven. The outer diameter of the oven is 14 mm and the total length with the cane (partially shown) is 870 mm.

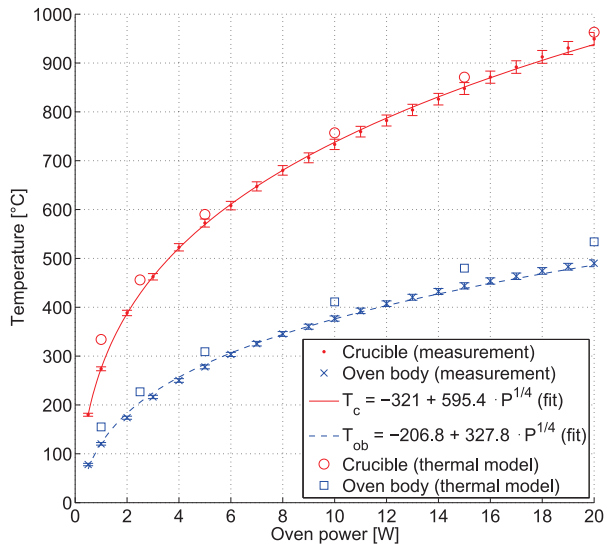

Figure 6: Measured crucible and oven outer body temperatures as a function of the oven input power. Temperatures predicted by the oven thermal model are also presented.

predicted by theory. The theoretical calculation is based on the Hertz-Knudsen equation for evaporation flux and an empirical formula for the estimation of the lead vapour pressure [12]. Figure 8 presents the long term behaviour of the lead output from the oven operated at a constant power of 12.5 W. Two phenomena observed with the measured evaporation rates are demonstrated in the figure. For the first 120 hours, the oven output decreases steadily over time with an average slope of about −0.3 unit-%/hour. This is then followed by instabilities characterized by sudden step-like decreases with plateaus of stable output between them. The latter behaviour could be connected to the dynamics and redistribution of the remaining lead inside the crucible, but further studies are necessary to give a more detailed explanation. The implication of the decreasing trend is that the oven power needs to be adjusted regularly to keep the evaporation rate at a constant value. This is indeed what is done in the GTS-LHC operation to maintain the extracted lead beam current at a constant level.

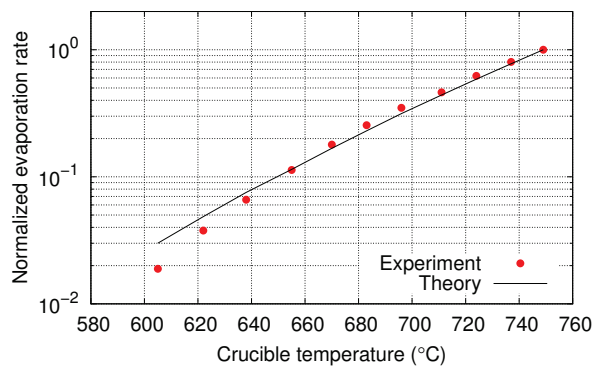

Figure 7: Measured and theoretically calculated normalized evaporation rates with varied crucible temperature. The temperature range for the measured data corresponds to oven powers between 6 W and 11 W.

ISBN 978-3-95450-186-1

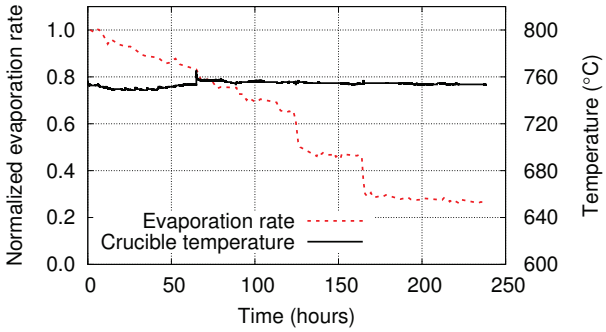

Figure 8: Evolution of the lead evaporation rate and crucible temperature over time with a constant oven heating power of 12.5 W.

A numerical thermal model of the miniature oven has been developed with the ANSYS simulation tools [13] to complement the measurements and provide insight into the temperature distributions inside the oven. The model is benchmarked against measured temperature behaviour at selected locations on the oven body and the model predictions agree well with the measured values (see Fig. 6).

Figure 9 presents calculated temperature distributions inside the oven with 10 W and 15 W heating powers. It is observed that a good temperature uniformity is achieved for the lead sample inside the crucible, while the tip of the oven remains significantly colder. The colder tip is presumed to be one of the issues contributing to the oven blockages experienced during operation.

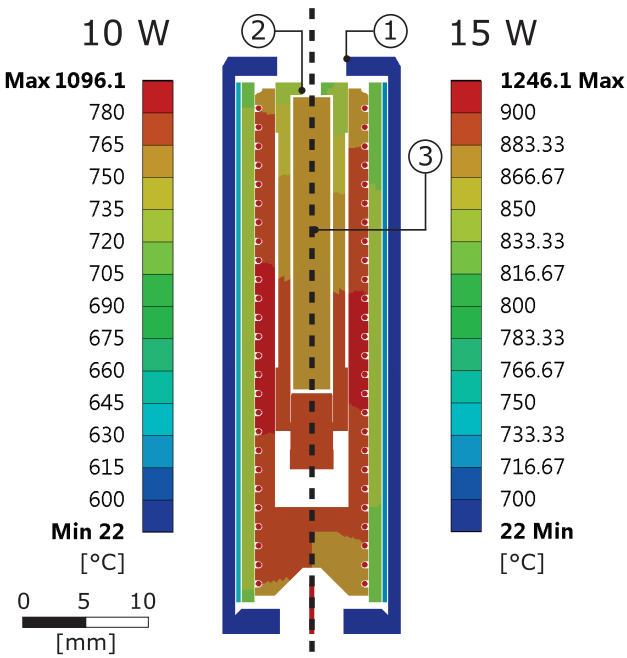

Figure 9: Simulated temperature distribution inside a lead filled oven with 10 W and 15 W powers. Temperatures at locations 1, 2 and 3 are 413, 729 and 756 °C for the 10 W case and 482, 833 and 870 °C for the 15 W case.

CONCLUSIONS

Thanks to the successful upgrade of the GTS-LHC extraction region, Linac3 is now routinely operated with improved beam currents and beam stability. The new beam conditions have also proven to be easier to reach and maintain owing to the increased flexibility in the ion source tuning. The present performance now fulfils the Linac3 output goal set in the LIU project, but studies to further improve the heavy ion performance will continue.

The double frequency experiments show that this method improves the high charge state ion currents also in afterglow mode. This combination is thus a viable option to improve ion source performance in applications where pulsed beams of high charge state ions are required. An improvement was also seen with Pb^{29+}, the main ion produced with GTS-LHC. Further studies are planned to assess if this method would be advantageous in normal Linac3 operation.

Concerning the miniature oven studies, the first basic characterization of the GTS-LHC oven has been carried out. The results show that the oven behaves mostly in the expected way in terms of temperature and evaporation rate trends. In addition, the thermal modelling has given the first hints to possible causes of the observed oven failure mechanisms. The future studies will focus on the details of these mechanisms and the different factors that impact the oven output behaviour (both magnitude and stability) during operation.

REFERENCES

[1] L. Dumas et al., in *Proc. of ECRIS'06*, Lanzhou, China, published in *HEP & NP, Vol.* 31, Suppl. 1, pp. 51-54 (2007).

[2] D. Hitz *et al.*, in *Proc. of ECRIS'02*, Jyväskylä, Finland (2002).

[3] V. Toivanen *et al.*, in *Proc. of ECRIS'14*, Nizhny Novgorod, Russia (2014).

[4] V. Toivanen *et al.*, *Rev. Sci. Instrum.* 87, 02B923 (2016).

[5] V. Toivanen *et al.*, *Rev. Sci. Instrum.* 87, 02B912 (2016).

[6] R. Vondrasek *et al.*, in *Proc. of ECRIS'02*, Jyväskylä, Finland (2002).

[7] R. Vondrasek *et al.*, *Rev. Sci. Instrum.* 77, 03A337 (2006).

[8] V. Toivanen *et al.*, "The effect of double frequency heating on the afterglow performance of the CERN GTS-LHC electron cyclotron resonance ion source", to be published.

[9] I. G. Brown (Ed.), "The physics and technology of ion sources", John Wiley & Sons, Inc., 2004.

[10] NIST Atomic Spectra Database, `http://physics.nist.gov/PhysRefData/ASD/ionEnergy.html`

[11] V. Skalyga *et al.*, *Phys. Plasmas* 22, 083509 (2015).

[12] D. R. Lide (Ed.), "CRC Handbook of Chemistry and Physics", 76th Edition, CRC Press, 1995.

[13] The official ANSYS simulation tools website, `http://www.ansys.com`

ISBN 978-3-95450-186-1